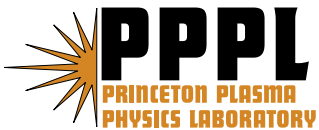# Princeton Plasma Physics Laboratory

Stochastic Ion Heating in a Field-reversed Configuration Geometry by Rotating Magnetic Fields

S.A. Cohen, A.S. Landsman,
and A.H. Glasser

June 2007

Princeton Plasma Physics Laboratory
Report Disclaimers

PPPL Report Availability

Princeton Plasma Physics Laboratory:

http://www.pppl.gov/techreports.cfm

Office of Scientific and Technical Information (OSTI):

http://www.osti.gov/bridge

Related Links:

U.S. Department of Energy

Office of Scientific and Technical Information

Fusion Links

Stochastic ion heating in a field-reversed configuration geometry by rotating magnetic fields

S.A. Cohen[1], A.S. Landsman[2], A.H. Glasser[3]

[1]Princeton Plasma Physics Laboratory, Princeton, NJ
[2]Naval Research Laboratory, Washington, DC
[3]Los Alamos National Laboratory, Los Alamos, NM

Abstract

Ion heating by application of rotating magnetic fields (RMF) to a prolate field-reversed configuration (FRC) is explored by analytical and numerical techniques. For odd-parity RMF (RMF_o), perturbation analysis shows ions in figure-8 orbits gain energy at resonances of the RMF_o frequency, ω_R, with the figure-8 orbital frequency, ω. Since figure-8 orbits tend to gain the most energy from the RMF and are unlikely to escape in the cusp region (where most losses occur), they are optimal candidates for rapid stochastic heating, as compared to cyclotron and betatron orbits. Comparisons are made between heating caused by even- and odd-parity RMFs and between heating in currently operating and in reactor-scale FRC devices.

I. INTRODUCTION

The field-reversed configuration (FRC), relevant to space-plasma,[1] plasma-processing,[2] spacecraft-propulsion,[3] and magnetic-confinement controlled-fusion[4] research, is an excellent system to explore particle dynamics in one, two, or three dimensions. Even with axial symmetry, a static FRC allows charged-particle orbits that are regular or ergodic,[5,6] affecting the confinement and stability of plasmas contained in it. Early studies of single-particle orbits in FRCs[7] assumed time invariance and spatial symmetries that reduced the problem to one or two dimensions, necessitating the existence of KAM surfaces and delimiting excursions in phase space. The addition of a rotating magnetic field (RMF,)[8] initially proposed to generate current,[9] breaks the angular invariance of the FRC, creating a three-dimensional system without bounding KAM surfaces, and opens the possibility for large excursions in phase space. These excursions may produce beneficial results, such as ion heating,[10,11] or detrimental ones, such as loss of confinement.

In this paper we present analytical and numerical studies of ion orbits in FRCs with RMFs applied. The goals are to understand the transition to chaotic orbits, to quantify the role of resonances in the non-linear growth and subsequent saturation of ion energy, to evaluate ion heating and single-particle confinement in present-day and future RMF/FRC experiments, and to make the first comparison between heating caused by two classes of rotating magnetic fields, even and odd parity.[12] We show that the same mechanism is responsible for the initial ion heating and its ultimate saturation.

Single-particle Hamiltonian dynamics, the technique employed in this study, is clearly appropriate at the low collisionality that exists in low-density space plasmas and high-temperature magnetic-confinement fusion devices. However, only one RMF/FRC device has achieved the very low Coulomb collisionality that fully justifies a Hamiltonian analysis.[13] As we shall show, notwithstanding, the time scale for RMF ion heating is often sufficiently short that the Hamiltonian approach remains valid and useful even for many collisional FRCs.

The analytical analyses herein are restricted to odd-parity RMFs (RMF_o) because of the existence of an invariant subspace that makes the equations tractable. We provide numerical analysis for both RMF_o and even-parity RMF (RMF_e).

Earlier papers[10,11] which examined the effects of low-amplitude RMF_os on ion heating in reactor-scale FRCs showed that the heating regime was $\omega_R \sim \omega_{ci} \gg \omega_{Rci}$, where ω_R is the

RMF_o angular frequency, $\omega_{ci} = qB_a/mc$ is the ion-cyclotron angular frequency in the axial field at the FRC's center, B_a, m is the ion mass, q is the ion charge, and $\omega_{Rci} = qB_R/mc$ is the ion-cyclotron angular frequency in an RMF of amplitude B_R. These papers reported significant ion heating – to fusion relevant energies – for $B_R/B_a \geq 5 \times 10^{-4}$. In this paper we consider that frequency regime in depth and also present results for $\omega_R \gg \omega_{ci}$, characteristic of one presently operating experiment.

Phase de-coherence of ion orbits, with respect to the periodic electric fields created by the RMF, is a necessary condition for heating, *i.e.*, velocity randomization. Nulls and strong gradients in the magnetic field provide locations for phase de-coherence. The existence of strong field gradients does not preclude the importance of ion-cyclotron resonances (ICRs) to ion heating. In this paper we show that ICRs are important, though with significant differences from the standard ICR picture. In numerical analyses we have seen that stronger heating occurs for ergodic figure-8 orbits than for the clearly resonant interaction between RMF and some cyclotron orbits. Cyclotron orbits may extract energy from the RMF over many periods, but only infrequently incur phase de-coherence, break-down of μ conservation, predominantly at the axial extremes of their orbits – unless they are near a phase-space separatix that allows their transition to figure-8 orbits. Figure-8 orbits cross the field-reversal region (twice) every orbit cycle, possibly losing phase coherence at each transversal. Because figure-8 orbits are representative of a large fraction of ions in hot fusion FRC plasmas, we focus on them. We have explained[14] why very high energy figure-8 orbits (and most betatron orbits) tend to interact regularly with RMF_o, leading, importantly, to a saturation of ion heating by RMF_o and a method for tuning ion energy.

As noted,[10,11] even for low B_R/B_a, appreciable ion heating occurs over a broad range of RMF_o frequency, $|\Omega| \equiv |\omega_R/\omega_{ci}| = 0.1 - 2$. (Positive Ω corresponds to RMF rotation in the direction predicted to drive current.[9]) We examine whether the broad range for Ω is due to heating at the changing fundamental ICR frequency as the ion moves through regions with different field strengths. The answer is no. Instead harmonic and sub-harmonic heating are occurring. The frequency of the figure-8 orbit is highly nonlinear, greatly changing with energy. As the energy of a figure-8 orbit decreases, the ratio $s \equiv \omega_R/\omega$ increases because the ion's frequency, ω, slows down as it gets closer to the phase-space separatrix, S_p. It follows that a set of resonances with the RMF_o occurs at $s = 1, 2, 3, ...$ as the ion trajectory gets closer to S_p and s increases.

The paper is organized as follows: In Section II, the model FRC and RMF fields and the associated Hamiltonians are presented. The RMF is assumed to be fully penetrated, as has been recently achieved in an experiment and as is desirable for ion heating throughout the FRC volume.[13] Section III provides detailed derivations for what was announced in a recent publication.[14] The energy gain from RMF_o is calculated for a single oscillation of a figure-8 ion in the $z = 0$ invariant subspace. This approximation is both useful and representative because many figure-8 orbits, especially higher energy ones, are confined close to the $z = 0$ plane.[15] The energy gained from the RMF_o field is then used to derive a condition for the transition from regular to ergodic orbits by applying the criterion for the exponential separation of trajectories, hence heating.[16] Section IV presents numerical results obtained with the RMF code.[11] First, we compare RMF_o heating of figure-8 ion orbits that fill the FRC volume with those constrained to the $z = 0$ subspace. Then, numerical studies for RMF_e heating in reactor-scale devices are presented and compared with RMF_o heating. Subsequently, results are presented for earlier and present-day RMF/FRC devices, some of which operate at $B_R/B_a \sim 0.5$. Section V concludes and summarizes.

II. BASIC EQUATIONS

We assume the confining magnetic field of the FRC inside the magnetic separatrix is described by the Solov'ev equilibrium,

$$\Phi = rA_\phi = \frac{B_a r^2}{2} \left(1 - \frac{r^2}{R^2} - \frac{z^2}{\kappa^2 R^2} \right) \tag{1}$$

with r the minor radius coordinate, z the axial coordinate, ϕ the azimuthal coordinate, R the FRC's separatrix radius at z = 0, Z the axial half length, $\kappa \equiv Z/R$ the elongation, $\vec{A}$ the vector potential, and Φ the flux function. In the numerical simulations, boundary conditions outside the separatrix are from Zakharov and Shafranov.[17]

Odd- and even-parity RMF are described by the vector potentials[11]

$$(A_r, A_z, A_\phi)_{odd} =$$

$$(2B_R/k)\,(I_0\,(\hat{\rho})\,cos(kz)sin(\psi), -I_1\,(\hat{\rho})\,sin(kz)sin(\psi), I_0\,(\hat{\rho})\,cos(kz)cos(\psi)) \tag{2}$$

$$(A_r, A_z, A_\phi)_{even} =$$

$$(2B_R/k)\,(I_0\,(\hat{\rho})\,sin(kz)sin(\psi), I_1\,(\hat{\rho})\,cos(kz)sin(\psi), I_0\,(\hat{\rho})\,sin(kz)cos(\psi)) \tag{3}$$

where $\psi = \phi - \omega_R t$, $\hat{\rho} = kr$, $k = l\pi/\kappa R$ is the axial wave number of the RMF, l is the axial mode number, $= 1$ in this study, and the I_m are modified Bessel functions. The resulting Hamiltonian,

$$H = \frac{1}{2}\left[(p_r - qA_r)^2 + (p_z - qA_z)^2 + \left(\frac{p_\phi}{r} - qA_\phi\right)^2\right],\qquad(4)$$

where p_i are the canonical momenta and A_ϕ denotes the sum of the RMF and FRC azimuthal vector potentials, is now three-dimensional, time-dependent and not conserved. The transformed Hamiltonian,[10] $\hat{K} = H - \omega_R p_\phi$, is conserved so that the dynamics are that of a three-dimensional autonomous system.

The shape of the effective potential energy surface on which an ion moves depends on z and on p_ϕ, a conserved quantity in the absence of RMF. Depending on the initial conditions of kinetic energy, momenta, and position, figure-8 orbits may be confined to the $z = 0$ subspace, or to a potential-well minimum above or below $z = 0$, or may oscillate across $z = 0$. In the case with no RMF and in the $z = 0$ subspace, the motion is one-dimensional and integrable.[7] The addition of RMF breaks the angular invariance, creating a nonlinear two-dimensional system.

Substituting the vector potentials into the Hamiltonian and using the Hamiltonian equations-of-motion, $\dot{q}_i = \partial H/\partial p_i$ and $\dot{p}_i = -\partial H/\partial q_i$, where q_i are the canonical coordinate variables, the equations-of-motion for a single ion inside the FRC in the presence of RMF are obtained. For RMF_o and initial conditions $z = 0$ and $p_z = 0$, it is straightforward to verify that $z = 0$ is an invariant subspace since the z-directed electric field created by RMF_o is zero there. (This is not the case with RMF_e.) The existence of an invariant subspace for RMF_o allows for an analytic analysis of trajectories. The question whether dynamics in this subspace is representative of dynamics throughout the FRC is addressed numerically in Section IV.

III.   ENERGY GAIN FROM RMF_o AND STOCHASTICITY OF ORBITS: z=0

We now calculate the RMF_o-induced energy gain of a figure-8 orbit in a single half period of its motion, starting with Eqs. (1), (2) and (4) evaluated in the $z = 0$ plane. Since the amplitude of the RMF_o magnetic field is small compared to the FRC's static magnetic field, an ion's trajectory is relatively unperturbed in a single oscillation along r. The energy gain in a single oscillation, caused the the RMF_o's electric field, is calculated as a first-order

correction to the one-dimensional motion along r. This one-dimensional motion is described by the Hamiltonian,

$$H = \frac{1}{2m} \left\{ p_r^2 + \left[\frac{p_\phi}{r} - \frac{qB_a}{2}r\left(1 - \frac{r^2}{R^2}\right) \right]^2 \right\},$$ (5)

showing that the motion is in a one-dimensional effective potential, $V(r)$. For the normalized canonical azimuthal momentum $\pi_\phi \equiv 2p_\phi/qB_aR^2 < 0.25$, the shape of the potential is a double well, corresponding to cyclotron orbits inside the phase-space separatrix, S_p, and to figure-8 orbits outside S_p. For $\pi_\phi > 0.25$, the potential is a single raised well, corresponding to betatron orbits.[15]

The figure-8 orbit is approximated by motion in a symmetric double well:

$$\rho \equiv \frac{r}{R} = \rho_0 + a_1 cos[\omega\,(t - t_0)] + a_2 cos[3\omega\,(t - t_0)],\ and\ v_r = \dot{r}.$$ (6)

The amplitudes of oscillation, a_1 and a_2, are determined by the total energy and by the shape of the double well; $0.577 < \rho_0 < 0.707$ with the upper limit corresponding to $\pi_\phi = 0.25$ and the lower limit to $\pi_\phi = 0$. In general, $a_1 \gg a_2$, especially at higher energies or higher values of p_ϕ.

The ion's energy change due to the RMF_o's electric field, $\vec{\mathcal{E}}$, is given by

$$\frac{dH}{dt} = q\vec{\mathcal{E}} \cdot \vec{v} = q\left(\mathcal{E}_r v_r + \mathcal{E}_\phi v_\phi\right),$$ (7)

with $\vec{\mathcal{E}} = -(1/c)(\partial \vec{A}/\partial t)$. Inside an elongated FRC, $l\pi/\kappa \leq 1$ and $\rho < 1$, allowing the RMF_o vector potential to be accurately approximated by

$$(A_r, A_z, A_\phi)_{odd} = (2B_R/k)\left[\left(1 + b_1\rho^2\right)sin(\phi - \omega_R t), 0, \left(1 + b_1\rho^2\right)cos(\phi - \omega_R t)\right],$$ (8)

with $b_1 = 0.25(kR)^2$. Using Eqs. (6)-(8), we obtain, after some algebra,

$$q\mathcal{E}_r v_r = -\omega H_0 \left(C_0 cos\left(\Psi\right) + \frac{1}{2}\sum_{n=1}^{9} C_n[sin\left(\Psi + (t - t_0)\,n\omega\right) - sin\left(\Psi - (t - t_0)\,n\omega\right)] \right)$$ (9)

where $\Psi = \phi - \omega_R t$ and the coefficients, C_n, depend on ρ_0, a_1 and a_2. The coefficients C_n are given in the appendix. H_0 in Eq. (9) is given by,

$$H_0 = R\omega_R\left(2qB_R/ck\right)b_1 = \frac{1}{2}mR^2\,kR\,\omega_{Rci}\,\omega_R,$$ (10)

where $kR = l\pi/\kappa$ was used. Since the amplitude of the RMF is relatively small, $B_R \ll B_a$, $\omega_{ci} \gg \omega_{Rci}$. For $\omega_R \sim \omega_{ci}$, $\omega_R \gg \omega_{Rci}$. Integrating Eq. (9) over a single half-oscillation in

6

r, we get the energy gain from the interaction with the r component of the RMF_o's electric field,

$$\triangle E_r = \int_{t=t_0}^{t_0+\pi/\omega} q\mathcal{E}_r v_r dt \tag{11}$$

$$\triangle E_r = \omega H_0 \left[-C_0 \frac{sin(\Psi_0)}{\omega_R} + \sum_{n=1}^{9} \frac{C_n}{2} \left(\frac{cos\left(\Psi_0 + (t-t_0)\,n\omega\right)}{\omega_R - n\omega} - \frac{cos\left(\Psi_0 - (t-t_0)\,n\omega\right)}{\omega_R + n\omega} \right) \right]_{t=t_0}^{t_0+\pi/\omega} \tag{12}$$

The biggest energy change occurs in the presence of a resonance between the RMF_o and the Fourier components of the oscillation. Since the RMF_o frequency is close to ω_{ci}, it is greater than the frequency of any figure-8 orbit inside the FRC. We are interested in resonances, i.e., $\omega_R/\omega = s$, where s is an integer. Substituting the limits into the Eq. (12), the energy change in a resonance due to the r component of the RMF_o vector potential becomes,

$$\triangle E_r = H_0 \left([F_0 + F_s]\,sin(\Psi_0) + \sum_{n=1}^{9,n\neq s} F_n(\omega)cos(\Psi_0) \right) \tag{13}$$

where $\Psi_0 = \phi - \omega_R t_0$ and the coefficients are given by:

$$F_n(\omega) = C_n \left[(-1) + (-1)^{s+n} \right] \frac{n}{s^2 - n^2}; \tag{14}$$

$$F_0 = -\frac{C_0}{s} \left[(-1) + (-1)^s \right]; \qquad \text{and} \qquad F_s = \frac{\pi}{2} C_s \tag{15}$$

Equations (13), (14) and (15) give the energy gain from the A_r component of the RMF_o in a single half-oscillation for an $\omega_R/\omega = s$ resonance.

A similar procedure is used to calculate the energy gain from the interaction of the ion with A_ϕ during a half-period of the ion's r motion. To calculate the $q\mathcal{E}_\phi v_\phi$ term in Eq. (7), we first need to determine v_ϕ. Equation (5) is for a one-dimensional system with a potential that is a function of r. Since the total kinetic energy in a static magnetic field is conserved, the potential term in Eq. (5) is actually the kinetic energy of azimuthal motion, giving

$$mv_\phi = \frac{p_\phi}{r} - \frac{qB_a}{2}r\left(1 - \frac{r^2}{R^2}\right). \tag{16}$$

Using the definitions of ρ and π_ϕ, v_ϕ may be written as

$$v_\phi = \frac{1}{2}\omega_{ci}R\left(\frac{\pi_\phi}{\rho} - \rho\left(1 - \rho^2\right)\right). \tag{17}$$

Expanding the π_ϕ/ρ term and keeping only terms up to the second order gives

$$v_\phi = \frac{1}{2}\omega_{ci}R\left[G_0 + G_2cos\left(2\omega\left(t - t_0\right)\right) + G_4cos\left(4\omega\left(t - t_0\right)\right)\right] \tag{18}$$

7

where

$$G_0 = \frac{\pi_\phi}{\rho_0} - \rho_0 + \rho_0^3 + \frac{a_1^2}{2}\left(\frac{\pi_\phi}{\rho_0^3} + 3\rho_0\right),$$ (19)

$$G_2 = \left(\frac{a_1^2}{2} + a_1 a_2\right)\left(\frac{\pi_\phi}{\rho_0^3} + 3\rho_0\right), \quad \text{and} \quad G_4 = a_1 a_2\left(\frac{\pi_\phi}{\rho_0^3} + 3\rho_0\right).$$ (20)

The coefficient G_0 gives the drift of the figure-8 orbit. Since the a_1^2 term makes a positive contribution to G_0, higher energy figure-8 orbits – which have a higher amplitude of oscillation, a_1 – have a greater counter-clockwise drift than lower energy ones.

The work done by the RMF due to interaction with azimuthal motion is given by

$$\triangle E_\phi = \int_{t=t_0}^{t_0+\pi/\omega} q\mathcal{E}_\phi v_\phi dt.$$ (21)

Using Eqs. (7), (8) and (18) in the above equation and following the same procedure as before, the energy change over a single half oscillation is given by

$$\triangle E_\phi = \omega_{ci} H_0 \left[K_0 \frac{cos(\Psi_0)}{\omega_R} + \sum_{n=1}^{8} \frac{K_n}{2}\left(\frac{cos\left(\Psi_0 + (t-t_0)\,n\omega\right)}{\omega_R - n\omega} + \frac{cos\left(\Psi_0 - (t-t_0)\,n\omega\right)}{\omega_R + n\omega}\right)\right]_{t=t_0}^{t_0+\pi/\omega}.$$ (22)

The K_n coefficients, functions of the azimuthal angular momentum and ion energy, are in the appendix. To find the energy change due to A_ϕ during a resonance, we follow the same procedure as was used to obtain Eq. (13),

$$\triangle E_\phi = H_0\left(Q_s(\omega)sin(\Psi_0) + \sum_{n=0}^{8,n\neq s} Q_n(\omega)cos(\Psi_0)\right),$$ (23)

where

$$Q_n(\omega) = K_n\left[(-1) + (-1)^{s+n}\right]\frac{s}{s^2 - n^2}\frac{\omega_{ci}}{\omega}$$ (24)

$$Q_s(\omega) = \frac{\pi}{2}\left(\frac{\omega_{ci}}{\omega}\right)K_s$$ (25)

From Eqs. (13) and (23), the total energy change in one r oscillation due to an interaction with a low-amplitude RMF_o is

$$\triangle E = H_0\left([F_0(\omega) + F_s(\omega) + Q_s(\omega)]sin(\Psi_0) + \sum_{n=0}^{9,n\neq s}[F_n(\omega) + Q_n(\omega)]cos(\Psi_0)\right),$$ (26)

where $F_8(\omega) = Q_9(\omega) = 0$. For odd resonances, coefficients $F_n(\omega)$ and $Q_n(\omega)$ are non-zero for even n values, so that Eq. (26) becomes

$$\triangle E_{s-odd} = H_0\left([F_0(\omega) + F_s(\omega) + Q_s(\omega)]sin(\Psi_0) + \sum_{n=0}^{4}[F_{2n}(\omega) + Q_{2n}(\omega)]cos(\Psi_0)\right).$$ (27)

8

Likewise, for even resonances, only odd values of n result in nonzero values of $F_n(\omega)$ and $Q_n(\omega)$, and $F_0 = 0$ [see Eq. (15)], so that Eq. (26) reduces to

$$\triangle E_{s-even} = H_0 \left([F_s(\omega) + Q_s(\omega)]sin(\Psi_0) + \sum_{n=0}^{4} [F_{2n+1}(\omega) + Q_{2n+1}(\omega)]cos(\Psi_0) \right). \quad (28)$$

The coefficients in Eqs. (27) and (28) depend on a_1 and a_2. The condition for confinement inside the FRC is: $\rho_0 + a_1 + a_2 < 1$ which leads to $a_1 < 0.35$. Since the value of a_2 is about an order of magnitude smaller than the value of a_1, higher n coefficients are significantly smaller. Thus K_6 is of order 10^{-4}, two orders of magnitude smaller than K_2. The biggest term in Eq. (26), used when considering odd resonances only, is

$$F_0(\omega) \approx (2/s)(a_1/b_1) \approx \frac{8}{s} \left(\frac{1}{kR} \right)^2. \quad (29)$$

All of the other terms are at least an order of magnitude smaller. Combined with the fact that C_n and K_n decrease exponentially as n increases, the greatest heating occurs for $s-odd$ resonances and $\Psi_0 = \pi/2$.

Using Eq. (27), where the dominant term is approximated by Eq. (29), we get the maximum approximate energy gain in a single oscillation:

$$max\triangle E_{odd} \approx \frac{8}{s} \left(\frac{1}{kR} \right)^2 H_0. \quad (30)$$

Approximating the total energy as $H \sim \frac{1}{2}m(R\omega a_1)^2$, $\omega_R \sim \omega_{ci}$, and $\omega_{Rci} = (B_R/B_a)\omega_{ci} \sim \omega s B_R/B_a$, the maximum relative energy fluctuation in a single oscillation is

$$\frac{max\triangle E_{odd}}{H} \approx \frac{8}{sa_1^2} (kR) \left(\frac{\omega_{Rci}}{\omega} \right) \left(\frac{\omega_R}{\omega} \right) \approx s \left(\frac{8}{a_1^2} \right) \left(\frac{1}{kR} \right) \left(\frac{B_R}{B_a} \right). \quad (31)$$

For the typical RMF wavelength and elongations used, i.e., $l = 1$ and $\kappa = 5$, $8\kappa/l\pi \sim 10$. With the amplitude of oscillation $a_1^2 \sim 10^{-1}$, the relative fluctuations in energy during an oscillation are of order

$$\frac{max\triangle E_{odd}}{H} \approx O \left(10^2 s \left(\frac{B_R}{B_a} \right) \right). \quad (32)$$

Equation (32) predicts significant energy fluctuations for figure-8 orbits over a single oscillation even for a relatively low relative RMF_o amplitude, $B_R/B_a \sim 10^{-3}$. The relative heating in Eq. (32) shows a linear dependence on the resonance, s, for odd values of s, and a linear dependence on B_R.

For $s-even$ resonances, the energy change is given by Eq. (28). It was found numerically that the odd coefficients, $F_{2n+1}(\omega)+Q_{2n+1}(\omega)$, in the summation in Eq. (28) are significantly smaller than the even coefficients $F_s(\omega) + Q_s(\omega)$, except for the $s = 8$ resonance, where it was found that F_8 and Q_8 are negligible compared to other coefficients. Using Eqs. (15), (25), (28) and $\omega_R = \omega_{ci}$, the maximum energy gain for the $s - even$ resonance can be approximated as

$$\triangle E_{s-even} \approx H_0 \left(F_s(\omega) + Q_s(\omega) \right) = \frac{\pi}{2} H_0 \left(C_s + sK_s \right), \tag{33}$$

where $max \left(C_s + sK_s \right) \sim O(1/2)$, so that

$$max \triangle E_{s-even} \approx \frac{1}{2} H_0. \tag{34}$$

Comparing Eqs. (30) and (34)

$$max \triangle E_{even} \approx \frac{s}{16} \left(kR \right)^2 max \triangle E_{odd}. \tag{35}$$

Using Eqs. (31) and (35), the percent energy fluctuation for an $s - even$ resonance becomes

$$\frac{max \triangle E_{even}}{H} \approx (kR) \left(\frac{s^2}{a_1^2} \right) \left(\frac{B_R}{B_a} \right) \sim O \left(10 s^2 \frac{B_R}{B_a} \right). \tag{36}$$

In summary, the energy gain for $s - even$ resonances has an s^2 dependence, while $s - odd$ energy gain has a linear dependence on s. Resonances with an odd value of s show better heating than $s - even$ resonances, especially at lower values of s, where ion energy is higher. (Since resonances with odd-s values show better heating, particularly at higher ion energies, the chaotic heating observed for figure-8 orbits at higher energies may result primarily from an overlap of odd-s resonances.)

Using the condition for exponential separation of trajectories,[16] we now investigate the ergodicity of ion trajectories, essential to stochastic heating. The change in energy over an oscillation can be used to map the dynamics,

$$E_{j+1} = E_j + \triangle E(t_j) \qquad \text{and} \qquad t_{j+1} = t_j + \frac{\pi}{\omega(E_{j+1})}, \tag{37}$$

where t_j is the time of the start of successive ion oscillations at $\rho = \rho_{max} \equiv \rho_0 + a_1$. Given the initial conditions, t_0 and E_0, Eq. (37) allows a recursive determination of E_j and t_j. $\triangle E(t_j)$ is given by Eq. (26),

$$\triangle E(t_j) = H_0 \left([F_0 + F_s + Q_s]sin(\Psi_j) + \sum_{n=0}^{9,n\neq s} [F_n + Q_n]cos(\Psi_j) \right), \tag{38}$$

10

where $\Psi_j = \phi - \omega_R t_j$. It was found numerically that stochastic heating for figure-8 orbits depends on the amplitude of the RMF_o. Figure 1 shows energy fluctuations for $B_R/B_a = 10^{-4}$ and 10^{-3}. For the larger B_R/B_a ratio, chaotic fluctuations of high amplitude, *ca.* $\pm 100\%$, are observed; there are only regular oscillations of order $\pm 12\%$ for the smaller ratio.
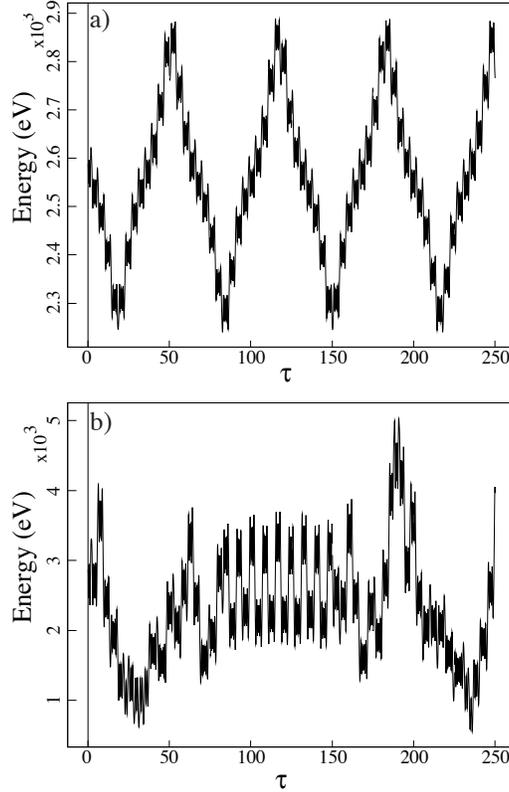

FIG. 1: Time evolution of ion energy in the RFRC under the influence of RMF_o. a) $B_R/B_a = 10^{-4}$. b) $B_R/B_a = 10^{-3}$.

To measure if the dynamics are chaotic we evaluate the exponential separation of trajectories using the strong-chaos condition[16]

$$\mathcal{K} = max \left| \frac{dt_{j+1}}{dt_j} - 1 \right| \gtrsim 1. \tag{39}$$

$\mathcal{K} > 1$ indicates exponential separation of trajectories, resulting in chaotic motion. Applying Eq. (39) to Eq. (37) yields

$$max \frac{\pi}{\omega^2(E)} \left| \frac{d\omega(E)}{dE} \frac{d\triangle E}{dt_j} \right| \gtrsim 1. \tag{40}$$

From Eq. (38), we obtain

$$\frac{d\triangle E}{dt_j} = -\omega_R H_0 \left([F_0(\omega) + F_s(\omega) + Q_s(\omega)]sin(\Psi_j) + \sum_{n=0}^{9,n\neq m} [F_n(\omega) + Q_n(\omega)]cos(\Psi_j) \right). \tag{41}$$

11

Using Eqs. (30) and (34), we get

$$max \left| \frac{d \triangle E_{odd}}{dt_j} \right| \approx \frac{8}{s} \left(\frac{1}{kR} \right)^2 (\omega_R H_0) \, ; \qquad max \left| \frac{d \triangle E_{even}}{dt_j} \right| \approx \frac{1}{2} (\omega_R H_0) \, . \qquad (42)$$

The above equations are to be substituted into Eq. (40) depending on whether the resonance, s, is even or odd.

To estimate $d\omega(E)/dE$, it is useful to work in dimensionless variables: $\tilde{H} = (m/b^2 R^2)H$, where $b = m\omega_{ci}/2$ and $p_\rho = p_r/bR$. The resulting dimensionless frequency, $\tilde{\omega} = m\omega/b = 2\omega/\omega_{ci}$ is in units of half the cyclotron frequency. In dimensionless variables,

$$\frac{d\omega(E)}{dE} = \frac{d\tilde{\omega}(\tilde{E})}{d\tilde{E}} \left(\frac{m}{b^2 R^2} \right) \left(\frac{b}{m} \right) = \left(\frac{1}{2} m \omega_{ci} R^2 \right)^{-1} \frac{d\tilde{\omega}(\tilde{E})}{d\tilde{E}} . \qquad (43)$$

Substituting Eqs. (42) and (43) into Eq. (40) and using Eq. (10), we get the following strong-chaos thresholds for odd and even resonances, respectively,

$$\mathcal{K}_{odd} \approx 8\pi s \left(\frac{1}{kR} \right) \left(\frac{B_R}{B_a} \right) \frac{d\tilde{\omega}(\tilde{E})}{d\tilde{E}} \quad \text{and} \qquad (44)$$

$$\mathcal{K}_{even} \approx \frac{\pi}{2} s^2 (kR) \left(\frac{B_R}{B_a} \right) \frac{d\tilde{\omega}(\tilde{E})}{d\tilde{E}} . \qquad (45)$$

Based on Eqs. (44) and (45), increasing the wavelength of the RMF would make $s - odd$ resonances more chaotic, while decreasing the heating from $s-even$ resonances. Since $s-odd$ resonances seem to be heated more effectively by the RMF (have higher $\mathcal{K}$), except for low energy figure-8 orbits when s is high, increasing the wavelength should increase stochastic heating for a range of B_R/B_a values. This is borne out by numerical simulation.

Figure 2 shows $d\tilde{\omega}(\tilde{E})/d\tilde{E}$ *vs.* $\tilde{E}$ for figure-8 orbits having $\pi_\phi = 0.15$. It was obtained by calculating ω's for a list of closely spaced E values, fitting those points to obtain a curve of ω *vs* E, then taking the derivative of that curve.

The value of s in a resonance decreases with increasing energy. There is a growth in $d\tilde{\omega}(\tilde{E})/d\tilde{E}$ as the energy decreases; for energies very close to S_p, $d\tilde{\omega}(\tilde{E})/d\tilde{E}$ grows as $(\tilde{E} - \tilde{E}_h)^{-5/6}$, where $\tilde{E}_h$ is the energy at S_p *i.e.*, at the peak separating the double potential wells. The continuing growth in $d\tilde{\omega}(\tilde{E})/d\tilde{E}$ approaching S_p corresponds to increasing non-linearity as the energy of a figure-8 orbit falls. A cyclotron orbit, on the other hand, does not transverse the potential barrier so that an energy increase has a much lesser affect on its orbital frequency, resulting in a more regular interaction with the RMF during a resonance.
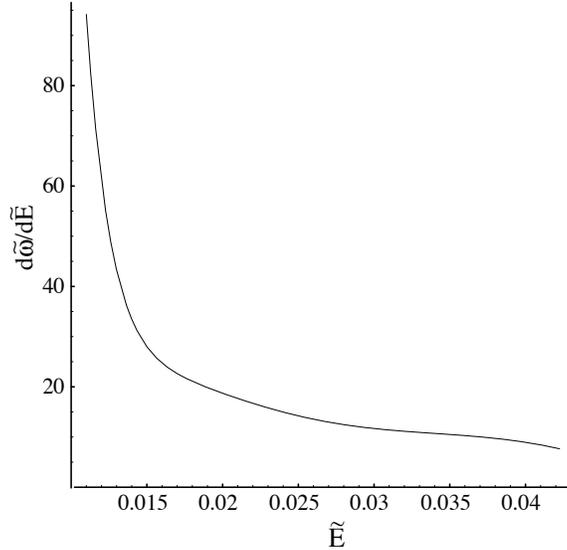
12

FIG. 2: $d\tilde{\omega}(\tilde{E})/d\tilde{E}$ vs $\tilde{E}$ for figure-8 orbits having $\pi_\phi = 0.15$.

The greatest rate of stochastic heating is expected to occur for lower energy figure-8 orbits where the values of s and $d\tilde{\omega}(\tilde{E})/d\tilde{E}$ are higher. As B_R is increased, the stochastic region above S_p will spread. Close to S_p, even very low amplitudes of B_R should produce chaotic orbits. Equations (44) and (45), combined with Fig. 2, can be used to estimate the relative amplitude of B_R needed to produce chaotic heating. For example, the $s = 3$ resonance occurs near $\tilde{E} \approx 0.0185$, corresponding to $d\tilde{\omega}(\tilde{E})/d\tilde{E} \approx 22$, see Fig. 2. Using Eq. (44) and $kR \sim 1$, for $\Omega \sim 1$, the assumption used in the derivation, chaotic trajectories are expected for all $s - odd$ resonances with $s \geq 3$ and $B_R/B_a \geq 5 \times 10^{-4}$. These findings approximately agree with the numerical findings. Changing the value of the normalized canonical azimuthal angular momentum, π_ϕ, changes the scale of $\tilde{E}$, but does not have a substantial effect on the value of $d\tilde{\omega}(\tilde{E})/d\tilde{E}$ at different resonances. Thus π_ϕ determines the energy range over which figure-8 orbits get heated, with greater energy range for lower values of π_ϕ, while not affecting the approximate structure of phase space. In Fig. 2, all $s > 4$ resonances are located to the left of $\tilde{E} \approx 0.013$, while lower s resonances are much more spread out. Thus the $s = 3$ resonance occurs around $\tilde{E} \approx 0.0185$ while all $s > 4$ resonances occur over the approximate interval of $\delta E = 0.003$. This leads to much greater chaos closer to S_p where the closely spaced resonances overlap. Thus, lower-energy figure-8 orbits are more chaotic and much better heated by the RMF than the higher energy ones.

IV. NUMERICAL RESULTS FOR ION HEATING

In this section we present numerical results not readily attainable by analytic means. (Our previous publication[14] provided numerical simulations that supported the analytic results announced therein and derived in detail herein, in Section III.) All simulations were performed with the RMF code[10,11] and assumed full RMF penetration, as recently achieved in experiment.[13] Simulations performed for reactor-scale FRCs used $R = 10$ cm, $B_a = 20$ kG, and $\kappa = 5$, previously named the reference FRC (RFRC).[10] Its size and axial field strength are about the smallest necessary to produce reactor-grade plasmas, that is, to contain deuterium ions with energies up to 200 keV, the upper limit of temperature needed for advanced, so-called *aneutronic*, fuels. (See Table I for the parameters of the all the FRC devices studied in this section.)

To test the validity of assumptions made in Section III, Section IV.A compares ion energy gained from RMF_o in the range $|\Omega| < 3$ for trajectories in the $z = 0$ subspace *versus* trajectories free to sample $z \neq 0$ regions of the RFRC volume. Section IV.B compares ion heating and confinement for RMF_e and RMF_o, again for $|\Omega| < 3$. This is representative of both the reactor regime and many RMF experiments that have operated over the last 40 years. Simulations range from reactor-relevant cases, where $B_R/B_a < 10^{-2}$, to $B_R/B_a \sim 0.5$, as encountered in many research-scale RMF devices and far from the validity range of the perturbation-technique analyses presented in Section III. Section IV.C presents results for $\Omega \gg 1$, characteristic of one currently operating device.[13]

A. RMF_o ion heating in and out of the $z = 0$ plane

Figure 3a) shows the time-averaged ion energy, $\langle E \rangle$, *versus* Ω for three values of RMF_o amplitude (2, 16 and 128 G) for ions initiated at 1-keV in the $z = 0$ plane of the RFRC with either initial $v_{z,0} = 0$ or $\neq 0$. Simulations were run to $\tau = (2\pi)5000/\omega_{ci}$. If an ion made a radial excursion to twice R or an axial excursion to twice κR, the ion was considered lost from the RFRC, the simulation terminated, and τ_{max} recorded. Qualitatively, the results for ion trajectories having $z = 0$ and $\neq 0$ are very similar, providing justification for $z = 0$ subspace analysis of ion heating presented in Section III.

For $B_R = 2$ G and both $v_{z,0} = 0$ and $\neq 0$, regular motion occurs when $-1 > \Omega > 1$ or $-0.1 < \Omega < 0.1$; the average energy stays within a few percent of the initial energy. For $0.1 < \Omega < 1$ and $-0.1 > \Omega > -1$, many ions experience some energy gain, to ~ 1.3 keV.

14

For $B_R = 16$ G, regular motion also occurs at high and low Ω, $|\Omega| > 1.7$, though even in these frequency regions $\langle E \rangle$ has climbed by $\sim 30\%$. Figure 3b), the inverse of the duration, τ_{max}, of each simulation *versus* Ω, shows that no particles were lost from these 4 simulations, $v_z = 0$ and $\neq 0$ and $B_R = 2$ and 16 G.
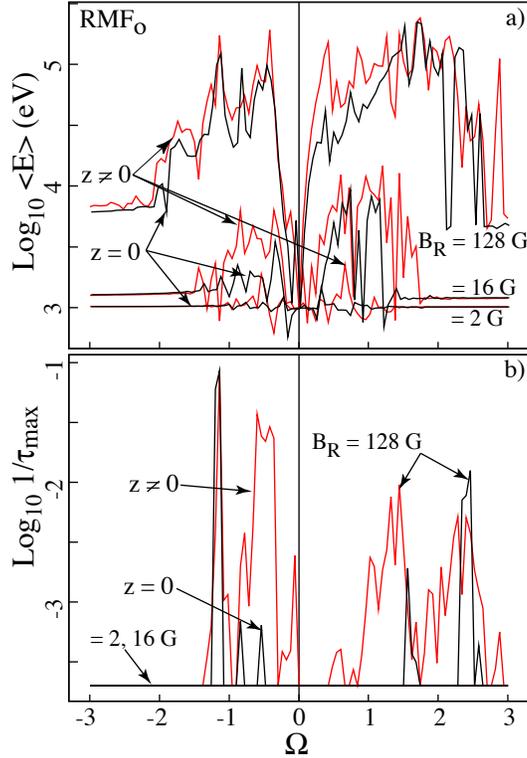

FIG. 3: (Color) Comparison of the Ω-dependence of ion heating and confinement under the influence of RMF_o for ions constrained to the RFRC $z = 0$ subspace (black lines) and those free to move throughout the RFRC (red lines). Three different RMF_o amplitudes were used: 2, 16, and 128 G.

On average, ions that strayed from the $z = 0$ plane achieved slightly lower average energies than those that remained in the $z = 0$ subspace but slightly higher peak energies (not shown). When heating occurs, the maximum energy achieved is about 3 times the average. The higher average energy achieved by ions in the $z = 0$ plane can be explained by the greater volume inside the phase-space separatrix for a given value of p_ϕ. The separatrix phase-space volume shrinks as ions move out of the $z = 0$ subplane. This means that for given energy along r, the figure-8 orbit has higher frequency, resulting in a lower s value and less nonlinearity, $d\tilde{\omega}/d\tilde{E}$. Based on Eqns. (44) and (45), this would lead to less chaotic motion, resulting in less heating as ions move out of the $z = 0$ subplane. Since the upper

15

limit on heating for figure-8 orbits is determined by the exponential separation of nearby trajectories, which depends on the s value and nonlinearity of orbits, the greatest heating occurs in the $z = 0$ subspace where the s value and the nonlinearity are the greatest for a given figure-8 orbit.

We have ascertained that little heating results from Speiser scattering at the FRC's axial extrema. Cyclotron orbits, generally of lower energy than figure-8 or betatron orbits, feel a force towards larger $|z|$, eventually entering a region where the barrier between the double wells is low enough for them to traverse it, thereby becoming figure-8 orbits. These are scattering events whereby ions may redistribute energy from the $\mathcal{E}_\phi$, $\mathcal{E}_z$ and $\mathcal{E}_r$ components of the RMF. But because cyclotron orbits are of lower energy when they arrive at the axial extrema, they have less energy to randomize, hence contribute less to the overall ion heating.

The three primary general features of Fig. 3a) can be understood from the discussion in Section III. Low heating in the range $|\Omega| < 0.1$ is due to the weak electric field, $\mathcal{E} \propto \omega_R B_R$. Saturation of heating for $0.15 < |\Omega| < 1.5$ is due to the reduction in s and $d\tilde{\omega}(\tilde{E})/d\tilde{E}$ at higher ion energy. The highest energy ions, betatron orbits, also interact regularly with the RMF, setting an upper limit for the heating of all ions in the FRC. The decrease in heating at $|\Omega| > 1$ occurs as the resonances, s, move to higher values and the energy gain coefficients decrease. An increase in RMF frequency requires different s resonances between the RMF and the figure-8 orbit to occur for higher energy figure-8 orbits, whose frequency is higher to match the higher frequency of the RMF. These resonances, however, are more separated in phase-space and are less chaotic, based on Eqns. (44) and (45), due to a fall in nonlinearity of a figure-8 orbit as the energy increases, *e.g.*, Fig. 2. In summary, there is an optimal range of RMF frequencies for which the greatest heating occurs as a result of interaction between the RMF and the figure-8 orbits, especially those orbits close to the phase-space separatrix. This range is bounded at its low end by the strength of the RMF electric field and at its upper end, near the cyclotron frequency, by overlap of resonances.

Figure 3b) shows that ions may be quickly ($t \sim 1$ μs) driven out of the RFRC even for $B_R/B_a \sim 0.006$. The maximum gyroradius of a 200 keV D^+ at $B_a = 20$ kG is $\rho_D \sim 5$ cm, which is larger than the distance between the O-point line and R. Note, though, that Fig. 3b) shows losses to be greater for ions not confined to the z = 0 subspace, so the gyroradius is not the complete explanation of the prompt losses. Viewing individual particle trajectories has shown that the losses predominantly occur in the cusp region of the external

magnetic field, near the X point, unique to the boundary conditions described in Ref. 16 and implemented in the RMF code. Fusion reactors which are intended to burn advanced fuels requiring very high ion temperatures might require somewhat higher B field and larger R than the RFRC. To reduce losses, they would benefit by operation at lower Ω values, below 0.5, and with the magnetic field shape tailored to avoid the aforementioned cusp. Fusion reaction products would not be well confined in a device as small as the RFRC. However, losses of these energetic particles is not inherently bad if high efficiency energy recovery systems are used. Moreover, the negative plasma potential that would result from fusion-product losses might improve confinement of the lower energy fuel ions.

The numerical finding that the losses occur predominantly near the cusp region rather than close to the $z = 0$ subplane shows an advantage for figure-8 heating. As previously mentioned, the largest fraction of figure-8 orbits is heated close to the $z = 0$ subplane where the nonlinearity of such orbits is highest. Since figure-8 orbits tend to stay close to the midplane, most of the losses near the cusp region are due to either low energy cyclotron orbits or orbits which have a significant z component in their velocities. As discussed in the next section, RMF heating along the z direction does not have a substantial affect on the over-all heating. This indicates that figure-8 orbits can be heated well by the interaction with the RMF_o, without resulting in significant losses. That is, the energy gains from RMF_o should not result in significant loss of confinement, provided the energy gains are primarily along the radial and azimuthal components of motion.

B. RMF_o and RMF_e heating for $|\Omega| < 3$

1. $B_R/B_a << 1$

We first consider deuteron heating in the RFRC, with $B_R/B_a < 0.02$. (Low B_R/B_a is desirable in a reactor to reduce circulating power; high B_R/B_a is desirable to aid stability and to increase heating and RMF penetration. $B_R/B_a \sim 0.01$ satisfies these criteria.) Simulations were run for $t = 10^4\pi/\omega_{ci}$, *i.e.*, $\tau = 5000$. Deuterons were initiated with 1 keV and $v_z \neq 0$ at $r = 0.85R$ in the $z = 0$ plane. If an ion made a radial excursion to twice R or an axial excursion to twice κR, the ion was considered lost from the RFRC and the simulation was terminated. The time-average D^+ energy, $\langle E \rangle$, maximum energy, E_{max}, and the duration of a simulation, τ_{max}, were tabulated. Typically, $E_{max} \simeq 3\langle E \rangle$.

Figures 4a) and 4d) show $\langle E \rangle$ as a function of RMF frequency for even and odd parity

respectively. The general features shown in Figs. 4a) and d) have been previously explained in Section IV.A and a previous publication.[14]
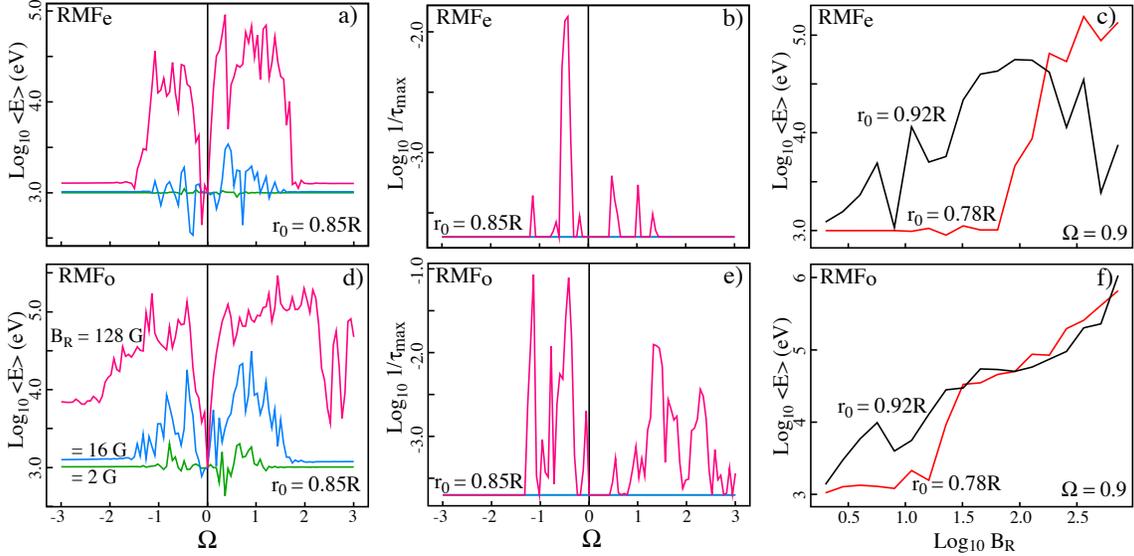

FIG. 4: (Color) Even- and odd-parity RMF ion heating in the RFRC, parts a) and d), and inverse confinement times, parts b) and e), *versus* Ω. In a), b), d) and e) three B_R values were used: 2 G (green), 16 G (blue), and 128 G (red). Parts c) and f) show the average energy *versus* B_R for two initial radial positions and fixed Ω.

Three RMF_o amplitudes were used: $B_R = 2, 16$ and 128 G. At $B_R = 2$ G, neither RMF_e nor RMF_o increased the ion energy substantially over the entire Ω range investigated, -3 to 3. When B_R was raised to 16 G, RMF_o did cause the average ion energy to increase above 3 keV if $-1 < \Omega < -0.2$ or $0.1 < \Omega < 1.3$. At $B_R = 16$ G, even parity produced lesser though still notable heating. Of the 400 deuterons initiated in each these even-parity and odd-parity simulations at $B_R = 2$ and 16 G, not one was lost due to a large radial or axial excursion, see Fig. 4b) and Fig. 4e). At $B_R = 128$ G, odd-parity RMF caused substantial heating, to $\langle E \rangle > 10^5$ eV, and even-parity RMF to $\langle E \rangle > 30$ keV. The frequency range for odd-parity heating was broader, showing heating to above 6 keV even for $-2 > \Omega > 2$. RMF_o at $B_R = 128$ G resulted in frequent deuteron losses, see fig. 4e). RMF_e at $B_R = 128$ G resulted in fewer losses, in part attributable to the smaller ρ_D at the lower attained energy. For both parities, loss rates were greater for $\Omega < 0$. RMF at negative Ω pushes π_ϕ to lower, eventually negative, values which results in axial losses across the separatix.[15] For even parity, loss rates were less for positive Ω.

18

Though RMF_e is predicted to open field lines and RMF_o should not, the loss rates shown in Fig. 4 imply that this effect is not important to ion particle confinement, at least at these low B_R/B_a values, large ion energies, short time scales, and large Ω values.

The effect of initial position and a wider range of B_R values on deuteron heating in the RFRC was explored. Figures 4 c) and f) show the average energy attained when the initial deuteron position was shift radially by $\sim \pm 10\%$, to $r_o/R = 0.78$ and 0.92, still outside the O-point line located at $r_o/\sqrt{2}$. Those initiated closer to the separatrix get heated at lower values of B_R. However, when $B_R > 100$ G, these ions are lost more readily and end up achieving a lower $\langle E \rangle$.

One feature in the RMF code is the ability to *shut off* $\mathcal{E}_\phi$, $\mathcal{E}_z$, and/or $\mathcal{E}_r$ arbitrarily, to explore which electric field components cause appreciable heating. Figure 5 shows results for both even and odd parity in the RFRC with $B_R = 128$ G. In these simulations deuterons were initiated at 100 eV out of the z = 0 plane at $r = 0.71R$. For even parity and $|\Omega| < 1$, Fig. 5a), shutting off $\mathcal{E}_z$ causes very little change in E_{max} while shutting off the $\mathcal{E}_r$ or $\mathcal{E}_\phi$ components drops the energy considerably, up to a factor of 10. Similarly, for RMF_o, $\mathcal{E}_z$ has little effect on E_{max} while $\mathcal{E}_\phi$ and $\mathcal{E}_r$ are both of considerable importance, though in different regions of Ω. There are a number of caveats. 1) Because heating is non-linear, simulations of the heating caused by separate components are not additive. 2) These conclusions are not to be extended to a different frequency (Ω) range, *e.g.*, for electrons. 3) The electric fields obtained by shutting off a particular component are not self-consistent. Notwithstanding, the results do support the interpretation that in a highly prolate FRC with RMF, Speiser scattering at the axial extrema is less important to heating than crossing the phase space separatrix.

A substantial amount of heating occurs due to an interaction between RMF_o and figure-8 orbits – a case we analytically investigated in the previous sections for the z = 0 subplane. As already mentioned, these orbits tend to stay close to the mid-plane, and are thus unlikely to gain substantial amounts of energy due to interaction with the z component of the electric field. This may, in part, explain the numerical results in Figure 5, indicating that the heating in the z component of ion dynamics is negligible for the over-all ion heating. Since figure-8 orbits also show good confinement, tending not to escape in the cusp region, these energy gains should remain inside the FRC rather than leaking out – at least on the time-scale that collisions can be neglected.
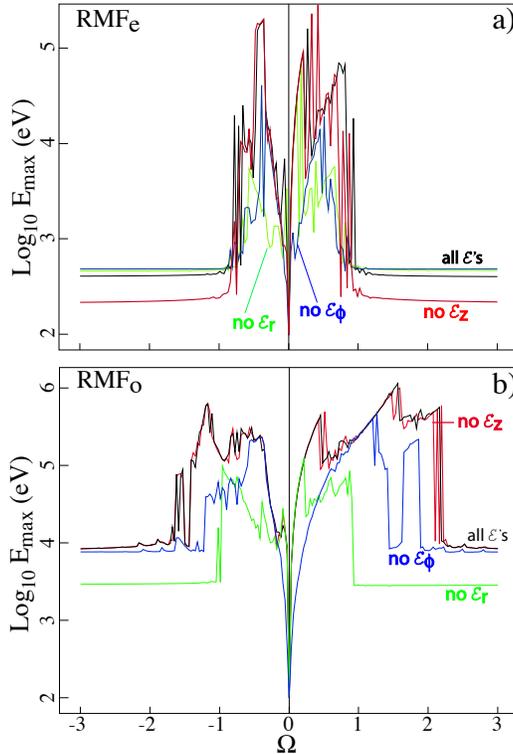
FIG. 5: (Color) Maximum D^+ energy achieved in the RFRC at $B_R = 128$ G *vs.* Ω for a) even- and b) odd-parity RMFs with various electric field, $\mathcal{E}$, components removed.

We conclude this sub-section with a closer look at low frequencies, $\Omega << 1$, outside the range of validity of earlier MHD RMF_e studies which assumed ions unmagnetized by B_R. Low Ω is a natural operating point for an RMF-driven FRC reactor because the relatively high density needed for fusion power and large R needed for confinement reduce the ω_R required for synchronous current drive, thus lowering Ω.

Figure 6 shows the maximum and average energies for D^+ and He_3^{+2} ions *versus* Ω_{He_3} in the RFRC at $B_R = 128$ G. (The frequency values for the D^+ data have been shifted by a factor of 4/3 so that each value of Ω_{He_3} corresponds to the same physical frequency for both the He_3^{+2} and the D^+.) Initiating ions at different radii, from 0.71R to 1.31R, had little effect on the results. The duration of each simulation was 3000τ. No ions were lost in this time period, as expected from Fig. 4. Though at each ω_R value, Ω for He_3, is less than for D, *i.e.*, $\Omega_{He_3} = 3/4\Omega_D$, at this value of B_R He_3^{+2} ions gets accelerated to about 50% higher average and maximum energy than D^+ ions. This ratio of ion energies will increase the *aneutronic* fusion component of a $D - He_3$ reactor.

To understand the reason for the higher energy, consider Fig. 7, which shows details
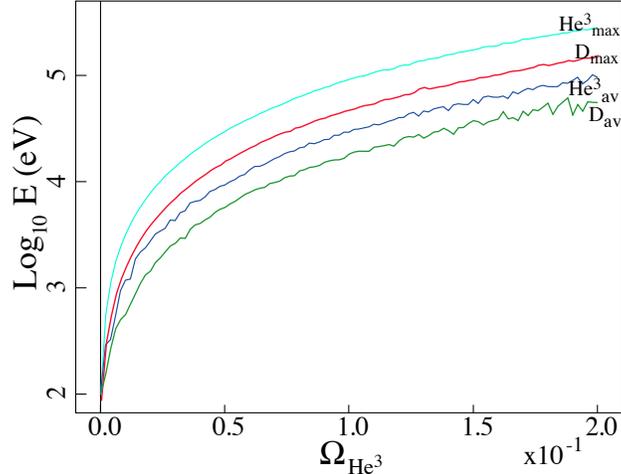
FIG. 6: (Color) Frequency dependence of the maximum and average energy of D^+ and He_3^{+2} ions heated by RMF_o in the RFRC. B_R was fixed at 128 G. The abscissa (frequency axis) for D has been multiplied by 4/3 so that the physical frequency on the abscissa is the same for both ions.

from one simulation of D^+ acceleration in the RFRC. Part a) shows D^+ energy *versus* time for $\Omega = 0.1$ and $B_R = 128$ G. (The data is color coded according to time.) Part b) is an expansion of the early time of part a). The energy is seen to rise and fall with regularity, reaching a peak of 32 keV. This type of behavior has already been observed for electrons and explained in detail.[11] It arises because electrons also have $\Omega << 1$. (In brief, the energy gain and loss are due to acceleration along the O-point line by the RMF_o-generated $\mathcal{E}_\phi$.) Part c) is a histogram of ion energy for the entire simulation. Part d) show the ion trajectory in the r-z cross section. Good confinement, particularly in the axial direction, is evident. Part e) shows two short sections of a D^+ trajectory, viewed along the z axis. The trajectory is predominantly a betatron orbit, with short-duration cyclotron behavior evident at x = 1, y = -6. When viewed in a frame-of-reference rotating at ω_R (part f), the ion is seen to move, on average, azimuthally with the RMF. This is also clear in part g). The blowup in part g) shows a 50τ segment of the azimuthal position; steps are evident. The "risers" of the steps have azimuthal angular speeds which are greater than ω_R; nevertheless, the average azimuthal angular ion speed is ω_R. (An ion's speed and energy only rise slightly with increasing B_R.) The same synchronous motion occurs for He_3^{+2}. Thus, at low Ω, heated ions — in betatron orbits — nearly co-rotate with the RMF, hence their energy is proportional to their mass.
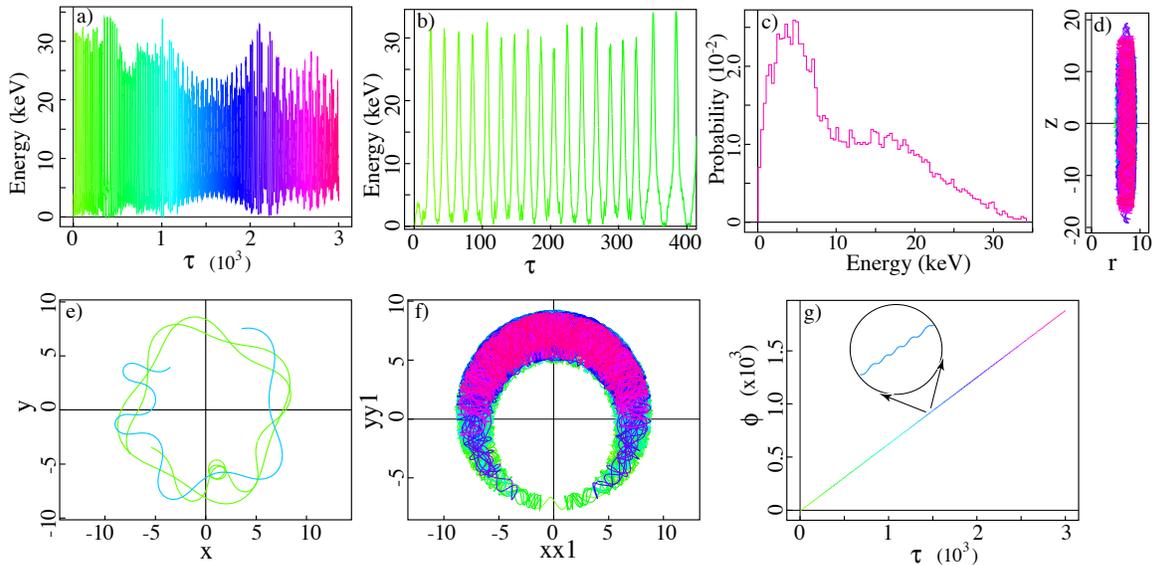
21

FIG. 7: (Color) D^+ heating by RMF_o in the RFRC: $\Omega = 0.1$, $B_R = 128$ G. a) and b) D^+ energy vs. time. c) D^+ energy distribution function. d) D^+ trajectory in r-z plane. e) segments of D^+ trajectory in x-y plane. f) D^+ trajectory in x-y plane rotating at ω_R. g) azimuthal position, ϕ, vs. time.

2. $B_R/B_a = 0.1 - 0.5$

We now consider $\Omega \sim 1$ ion heating at higher B_R/B_a values, relevant to some currently operating machines, particularly TCS. The TCS parameters in Table I, taken from a publication,[18] are for one of its best performing RMF_e discharges, having achieved a steady-state electron temperature near 50 eV at $\bar{n}_e = 1.3 \times 10^{13}$ cm^{-3}. Measurements showed that the RMF_e only penetrated ~ 10 cm into the plasma, to about the O-point line. To take this behavior partially into account, the initial D^+ radius, r_i, used in the RMF simulations was outside the O point. Figure 8 shows the maximum energy achieved as well as the inverse of the ion confinement time, in units of $\tau \sim 6$ μs. At B_R values consistent with the experiment, ca. 50 G, most ions were accelerated quickly to 1 keV and promptly lost, i.e., in a few RMF_e cycles, ca. 20 μs. The strength of the RMF-generated electric field is large, ~ 2 kV/m. At $E = 2$ keV, the ion gyroradius is over 40 cm, hence prompt loss is readily understandable. Collisions with ions and neutrals and electron drag will reduce this effect but we estimate that a consider number of the ions are still accelerated to near keV energy and lost. This predicted phenomenon, keV ions impacting the TCS wall, should be considered when trying to evaluate the source of impurities in TCS discharges.
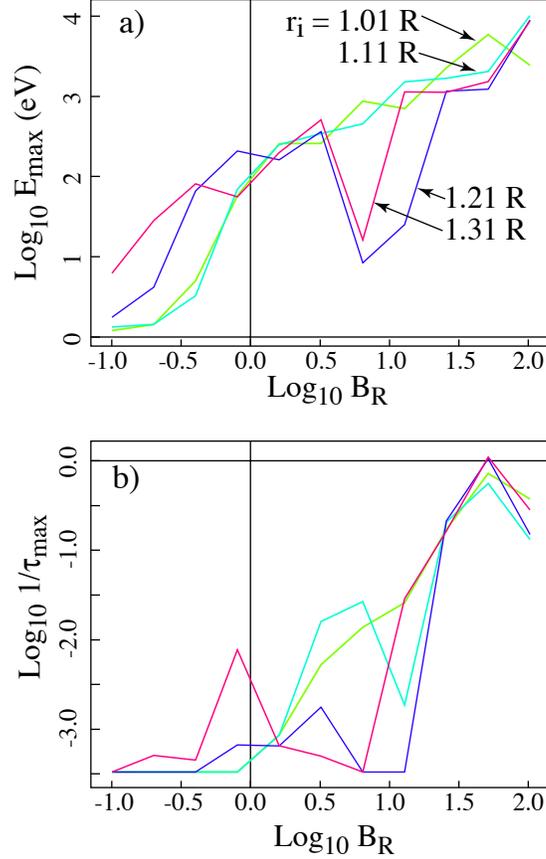
FIG. 8: (Color) a) *Log_10 E_max* and b) and *Log_10 (1/τ_max)* *versus* even-parity RMF strength, B_R, for TCS.

We have made a limited number of RMF simulations to search for an RMF parameter space in TCS where ion losses are less rapid. Going to a moderately higher Ω, from 1.55 to near 10, even while maintaining $B_R = 50$ G , results in far lower ion losses. Operation at higher RMF_e frequency would require lower plasma density to be consistent with current drive parameters.

C. $\Omega \gg 1$ and $B_R/B_a \sim 0.1$

A limited number of simulations were made for the parameter range of the PFRC experiment. Using the parameters in Table I, hydrogen ions were lost within a few τ's if the cusp boundary condition[17] was implemented. However, adding a mirror field representative of the PFRC device increased the ion confinement time to above 30 μs and predicted an average ion energy of ~ 15 eV. The experiment[13], however, shows average hydrogen neutral energies near 0.5 eV. This is consistent with a high charge-exchange rate at the large neutral density present in the PFRC.

TABLE I: Parameters of PFRC, TCS and RFRC.

Parameters	PFRC	TCS	RFRC
$_pB_0$ (kG)	0.12	0.13	20
Mirror ratio, R_m	60	4	10
Z (cm)	15	120	50
Flux conserver radius, R_{FC} (cm)	4	47	20
Plasma radius, R (cm)	3	37	10
B_R (G)	10	50	400
$B_R/_pB_0$	0.08	0.39	0.02
Working gas	H_2	D_2	D_2
n_e (10^{13} cm^{-3})	0.13	1.3	15
Fill pressure, p_n (mT)	1	2	
RF heating power (kW)	5	1000	500
T_e (eV)	200	50	10^4
$_mE_i$ (eV) measured	0.6	2	
$_cE_i$ (eV) calculated	0.9	$10^3 - 10^4$	5×10^4
ω_R (10^6 rad/s)	88	0.96	11
ω_{pe} (10^{11} rad/s)	0.6	2	7
ω_{ce} (10^9 rad/s)	2	2	350
ω_{ci} (10^6 rad/s)	1.15	0.62	90
$\Omega \equiv \omega_R/\omega_{ci}$	76	1.55	0.15
$\nu_{e,n}$	4×10^5	2×10^6	3×10^2
$\nu_{e,i}$	2×10^4	1.6×10^6	6×10^3
$\nu_{i,i}$ at E_i measured	2×10^6	10^7	
Ion gyroradius (cm) at $_mE_i$	0.8	2	
3.6 MeV α gyroradius, ρ_α, (cm)			10
Electron gyroradius (cm)	0.02	0.01	0.01
Penetration criterion, γ_c/λ,[19]	100	13	140

V.   CONCLUSION

The conditions for ion heating in the FRC in the presence of rotating magnetic fields were investigated using analysis and numerical simulation. Both odd- and even-parity RMFs were considered using numerics. It was found that odd-parity fields show greater heating for a wider range of RMF frequencies, Ω. Since figure-8 orbits are heated by RMF field more than other orbits classes, we analyzed the heating of a figure-8 orbit in the miplane in the presence of odd-parity RMF. It was found that even low amplitude fields, $B_R/B_a \sim 10^{-3}$, can result in significant energy gains, particularly in the case of resonant figure-8 orbits

24

that are close to the phase-space separatrix. The results explain the efficacious heating for $0.1 < \Omega < 1.3$ frequency range by resonances of the RMF with the lower energy figure-8 orbits. A criterion for strong chaos was used to show that such orbits are more chaotic due to increased nonlinearity, $d\tilde{\omega}(\tilde{E})/d\tilde{E}$ and a higher s value. Numerical simulations show that the heating in $z = 0$ subplane and throughout the FRC is similar, allowing for the extension of the analytic results obtained for heating in the midplane. Analysis indicates that the greatest heating of figure-8 orbits occurs close to the midplane – a result that agrees with numerics. Based on simulations, it was found that most of the ions escape in the cusp region. The z component of the RMF electric fields, which may contribute to cusp losses by accelerating the ions axially, was found to have little impact on heating. Since figure-8 orbits tend to stay confined close to the midplane and are unlikely to escape along the cusp or gain much energy from the z component of the electric fields, the numerical results futher validate the use of figure-8 orbits as optimal for FRC heating. Simulations for the TCS experiment show rapid ion acceleration to keV energies and prompt loss because $\Omega \sim 1$ and $B_R/B_a \sim 0.3$.

APPENDIX A: Energy-gain expansion coefficients

The coefficients are given by:

$$C_0 = (a_1/b_1) + \rho_0^2 + (1/2)\left(a_1^2 + a_2^2\right) \tag{A1}$$

$$C_1 = -(1/4)a_1^2\left(a_1 - a_2\right); \qquad C_2 = \rho_0 a_1\left(a_1 + 2a_2\right) \tag{A2}$$

$$C_3 = (1/4)\left(a_1^3 - 3a_2^3\right); \qquad C_4 = 4\rho_0 a_1 a_2; \qquad C_5 = (5/4)\left(a_1 a_2\right)\left(a_1 + a_2\right) \tag{A3}$$

$$C_6 = 3\rho_0 a_2^2; \qquad C_7 = (7/4)a_2^2 a_1 \tag{A4}$$

$$C_8 = 0; \qquad C_9 = (3/4)a_2^3 \tag{A5}$$

$$K_0 = (1/2)G_0 C_0 + (1/4)G_2\left(a_1^2/2 + a_1 a_2\right) + (1/4)G_4(a_1 a_2) \tag{A6}$$

$$K_1 = G_0(\rho_0 a_1) + G_2\rho_0\left(a_1/2 + a_2/2\right) + (1/2)G_4\rho_0 a_2 \tag{A7}$$

$$K_2 = G_0\left(a_1^2/4 + a_1 a_2/2\right) + G_2\left(C_0/2 + a_1 a_2/4\right) + (1/2)G_4\left(a_1/2 + a_2/2\right)^2 \tag{A8}$$

$$K_3 = G_0(\rho_0 a_2) + (1/2)G_2(\rho_0 a_1) + (1/2)G_4(\rho_0 a_1) \tag{A9}$$

$$K_4 = G_0(a_1 a_2/2) + (1/2)G_2 \left(a_1/2 + a_2/2\right)^2 + (1/2)G_4 C_0 \tag{A10}$$

$$K_5 = G_2(\rho_0 a_2/2) + G_4(\rho_0 a_1/2) \tag{A11}$$

$$K_6 = G_0(a_2^2/4) + G_2(a_1 a_2/4) + G_4 \left(a_1^2/8 + a_1 a_2/4\right) \tag{A12}$$

$$K_7 = (1/2)G_4(\rho_0 a_2); \qquad K_8 = G_2(a_2^2/8) + G_4(a_1 a_2/4) \tag{A13}$$

[1] J. Chen, *J. Geophys. Res.* **97**, 15011 (1992).

[2] I. Yu. Kostukov and J.M. Rax, *Phys. Plasmas* **7**, 185 (2000).

[3] A.L. Hoffman, H.Y.Y. Guo, J.T. Slough, S.J. Tobin, L.S. Schrank, W.A Reass, and G.A Wurden, *Fus. Sci. and Technol.* **41**, 92 (2002).

[4] M. Tuszewski, *Nucl. Fusion* **28**, 2033 (1988).

[5] J. M. Finn and R. N. Sudan, *Nucl. Fusion* **22**, 1443 (1982).

[6] A. S. Landsman, S. A. Cohen, M. Edelman, and G. M. Zaslavsky, *Comm. Nonlinear Sci. and Numer. Simul.* **10**, 617 (2005).

[7] M. Y. Wang and G. H. Miley, *Nucl. Fusion* **19**, 39 (1979).

[8] W. N. Hugrass, I. R. Jones, and M. G. R. Phillips, *Nucl. Fusion* **19**, 1546 (1979).

[9] H. A. Blevin and P. C. Thonemann, *Nucl. Fusion Suppl.* **1**, 55 (1962).

[10] S. A. Cohen and A. H. Glasser, *Phys. Rev. Lett.* **85**, 5114 (2000).

[11] A. H. Glasser and S. A. Cohen, *Phys. Plasmas* **9**, 2093 (2002).

[12] S. A. Cohen and R. D. Milroy, *Phys. Plasmas* **7**, 2539 (2000).

[13] S.A. Cohen, B. Berlinger, A. Brooks, C. Brunkhorst, N. Ferraro, D.P. Lundberg, A. Roach, and A.H. Glasser, *Phys. Rev. Lett.* **98**, 145002 (2007).

[14] A. S. Landsman, S. A. Cohen, and A. H. Glasser, *Phys. Rev. Lett.* **96**, 015002 (2006).

[15] A. S. Landsman, S. A. Cohen, and A. H. Glasser, *Phys. Plasmas* **11**, 947 (2004).

[16] G. M. Zaslavsky, *Physics of chaos in Hamiltonian systems* (Imperial College Press, London, 1998) p. 33.

[17] L.E. Zakharov and V.D. Shafranov, "Equilibrium of Current-carrying Plasmas in Toroidal Configurations" in *Reviews of Plasma Physics* **11**, M.A. Leontovitch, ed., (Consultants Bureau, New York, 1986) p. 153.

[18] A. L. Hoffman, H. Y. Guo, K.E. Miller, and R.D. Milroy, *Phys. Plasmas* **13**, 012507 (2006).

[19] R. D. Milroy, *Phys. Plasmas* **6**, 2771 (1999).